remote sensing

MDPI

Article

Intra-Annual Variabilities of *Rubus caesius* L. Discrimination on Hyperspectral and LiDAR Data

Anna Jarocińska [1,*], Dominik Kopeć [2,3], Barbara Tokarska-Guzik [4] and Edwin Raczko [1]

1 Department of Geoinformatics, Cartography and Remote Sensing, Chair of Geomatics and Information Systems, Faculty of Geography and Regional Studies, University of Warsaw, 00-927 Warsaw, Poland; edwin.raczko@uw.edu.pl
2 Department of Biogeography, Paleoecology and Nature Conservation, Faculty of Biology and Environmental, University of Lodz, 90-237 Łódź, Poland; dominik.kopec@biol.uni.lodz.pl
3 MGGP Aero sp. z o.o., 33-100 Tarnów, Poland
4 Research Team of Botany and Nature Protection, Institute of Biology, Biotechnology and Environmental Protection, Faculty of Natural Sciences, University of Silesia in Katowice, 40-032 Katowice, Poland; barbara.tokarska-guzik@us.edu.pl
* Correspondence: ajarocinska@uw.edu.pl; Tel.: +48-606491444

Abstract: The study was focused on a plant native to Poland, the European dewberry *Rubus caesius* L., which is a species with the ability to become excessively abundant within its original range, potentially causing significant changes in ecosystems, including biodiversity loss. Monitoring plant distributions over large areas requires mapping that is fast, reliable, and repeatable. For *Rubus*, different types of data were successfully used for classification, but most of the studies used data with a very high spectral resolution. The aim of this study was to indicate, using hyperspectral and Light Detection and Ranging (LiDAR) data, the main functional trait crucial for *R. caesius* differentiation from non-*Rubus*. This analysis was carried out with consideration of the seasonal variability and different percentages of *R. caesius* in the vegetation patches. The analysis was based on hyperspectral HySpex images and Airborne Laser Scanning (ALS) products. Data were acquired during three campaigns: early summer, summer, and autumn. Differentiation based on Linear Discriminate Analysis (LDA) and Non-Parametric Multivariate Analysis of Variance (NPMANOVA) analysis was successful for each of the analysed campaigns using optical data, but the ALS data were less useful for identification. The analysis indicated that selected spectral ranges (VIS, red-edge, and parts of the NIR and possibly SWIR ranges) can be useful for differentiating *R. caesius* from non-*Rubus*. The most useful indices were ARI1, CRI1, ARVI, GDVI, CAI, NDNI, and MRESR. The obtained results indicate that it is possible to classify *R. caesius* using images with lower spectral resolution than hyperspectral data.

Keywords: dewberry; HySpex; imaging spectroscopy; vegetation indices; airborne laser scanning; non-parametric multivariate analysis of variance; linear discriminant analysis

Citation: Jarocińska, A.; Kopeć, D.; Tokarska-Guzik, B.; Raczko, E. Intra-Annual Variabilities of *Rubus caesius* L. Discrimination on Hyperspectral and LiDAR Data. *Remote Sens.* **2021**, *13*, 107. https://doi.org/10.3390/rs13010107

Received: 13 November 2020
Accepted: 28 December 2020
Published: 31 December 2020

1. Introduction

Growing global phenomena such as land-use changes or habitat fragmentation, and the accompanying climate change yielding changes in the ecological and geographical ranges of species, lead to biodiversity loss [1–5]. Plant species that spread on a massive scale beyond their original geographical ranges and native species becoming excessively abundant within their original ranges often cause significant changes in ecosystems, including biodiversity loss [6–8].

The present study is focused on a *Rubus caesius* L. species from the brambles genus (*Rubus*), which has traits that favour spreading, such as low trophic requirements and quick adaptation to changing habitat conditions. In addition, by competing with other resident species, brambles limit the populations of other species by competition and strongly modu-

late species interactions and community composition, leading to a decline in biodiversity in the affected habitats [9–12], including protected in Europe Natura 2000 habitats.

Rubus caesius L. (European dewberry, *R. caesius*) belongs to the large and diverse genus of *Rubus* (bramble) within the Rosaceae family, covering about 430 and 750 species [13]. Numerous species and infrageneric taxa have been subsequently recognised, recently reaching about 1500 species worldwide [14], depending on the taxonomic approach. This plant is a half-bush reaching a height of 0.5–2 m with shoots lying on the ground. The main identification features of this species include the morphology of its stems (usually slender and pruinose, with short, slender, and needle-like prickles), leaves (three-foliate with broad-based, gibbous lateral leaflets; the stipules are broadly lanceolate) and generative organs: flowers (white flowers, appearing both on previous-year and current-year twigs, gathered in corymbose inflorescences) and fruit (ripe black drupeles pruinose) [15].

Rubus caesius grows in forest and shrub communities with natural features (mostly in riverside riparian woodland), as well as at the edges of forests but much more often in meadows (formed in the habitats of ancient riparian forests) and ruderal communities (Figure 1) [15–17]. Dewberry is also a threat to non-forest natural habitats [16]. In many cases, the plant creates large, homogeneous patches. It also may cause problems as a weed, e.g., in maize and winter wheat [18,19] or other cereal crops (own observations).

Figure 1. Images of *Rubus caesius* taken at the study area acquired in summer (second campaign, C2).

R. caesius depends mainly on vegetative reproduction using the buds on its roots and creeping stems and less on its seeds. Its developmental phases correspond to the seasons of the year, but *R. caesius* tends to flower throughout much of the growing season [20]. Thus, vegetative growth occurs from early spring, with the flowering and fruiting phase ranging from May to September. The first-year canes or shoots of *R. caesius* are pedunculated, round, straight, thin, glabrous, or slightly pubescent, waxy frosted, herbaceous bluish, glaucous, and tinged red where exposed to sun. Two-year-old shoots are partly woody at the base, branched, bloom and bear fruit, and usually die after two seasons. The leaves contain tannins, flavonoids, anthocyanin dyes, organic acids, vitamin C, vitamin B, vitamin P, inositol, and pectin [21]; moreover, *Rubus caesius* leaf extracts have medicinal value [22,23]. A detailed description of species variability during the growing season is described in Section 3.2.

Rubus caesius is widespread throughout Europe and Western and Central Asia [15] but is also observed outside its original range in North America [24]. In methodological guides prepared for the purposes of monitoring of specific protected ecosystems, *Rubus* is listed among the expansive species that threaten the following non-forest Natura 2000 habitats: xerothermic grasslands *Festuco-Brometea* (code 6210) [25], mountain yellow *Trisetum* and Bent-grass hay meadows (*Polygono Trisetion* and *Arrhenatherion*) (code 6520), lowland hay

meadows (*Arrhenatherion*) (code 6510) [26,27], and also species-rich *Nardus* grasslands on siliceous substrates in mountain areas (and submountain areas, in Continental Europe) (code 6230) [27] and dry heath communities *Calluno-Genistion*, *Pohlio-Callunion*, *Calluno-Arctostaphylion* (code 4030) [28]. In the case of the meadows, the presence of *Rubus* most often testified to the absence of mowing. In the Natura 2000 European Ecological Network, invasive alien species (IAS) is one of the key parameters that provides information about the level of status conservation of every habitat [29]. Hence, quick identification of the presence of this species is essential for the effective protection of many natural habitats. To support assessments of the effects of global change on ecosystems, an important task is to develop easy methods and tools for data integration, processing, storage, and analysis. Detecting the species is the first step in monitoring and should be done as simply as possible.

For the *Rubus* genus, different types of data were successfully used for classification. Bramble *R. fruticosus* was effectively monitored using HyMap hyperspectral data with high accuracy (the best Overall Accuracy (OA) was 92%; kappa 0.715) [30]. Data were acquired in November (spring in Australia). HySpex images were used to classify three different expansive species including *Rubus* spp.; the F1 for the best dataset was equal to 0.97 for the Support Vector Machine classifier and 0.95 for Random Forest [31]. The Himalayan Giant bramble *Rubus armeniacus* was successfully classified (OA from 61.8% to 76.4%) using spectral bands from the Compact Airborne Spectrographic Imager (CASI) and Light Detection and Ranging (LiDAR) [32]. The same spectral CASI data combined with LiDAR-derived layers were used in the classification, where the OA was equal to 87.8% and the kappa coefficient was 0.75 [33]. The species *Rubus caesius* was successfully classified on the basis of the CASI and LiDAR data, where the User Accuracy (UA) for the class was 82%, and the Producer Accuracy (PA) was 58% [34].

Some of the multispectral satellite data were also tested for *Rubus* mapping. Satellite Landsat 8 and Sentinel-2 were used to identify the American bramble (*Rubus cuneifolius*) [35]. As a result, Sentinel-2 out-performed Landsat 8 in all seasons, with summer showing the highest accuracy (OA 77%, PA 80%, UA 45%). The Sentinel-2 bands of NIR, red-edge, and SWIR were crucial for increasing mapping accuracy. The images from SPOT 5 acquired in different seasons were used to identify *Rubus cuneifolius* as an invasive species in northern KwaZulu-Natal [36]. Different classifiers and approaches were tested, and the best OA for *Rubus* was 82% with a kappa of 0.71.

Based on this information, dewberry can be successfully identified, but it is necessary to collect optimal data. The high spectral and radiometric resolution makes it possible to identify brambles with high accuracy, but it is also possible to map large patches of *Rubus* using satellite Sentinel-2 images. For high spectral resolution data, much information must be processed over a long time using dedicated algorithms. Identification of the species through monitoring must also be precise and as fast and easy as possible. Thus, it is crucial to define the remote sensing data for proper identification.

2. Aim of the Study

Monitoring vegetation areas requires species identification that is fast, reliable, and repeatable. Dewberry classification is possible, which was proven in the studies mentioned above. At the same time, it has not yet been determined which remote sensing data are necessary for proper classification. The aim of this study is to define the following:

- What type of remote sensing data differentiates *R. caesius* from non-*Rubus* depending on its coverage and the date used for image acquisition;
- Which remote sensing data (spectral bands, calculated indices, and structural metrics derived from ALS) are the most discriminant of *R. caesius* under different growth and pigmentation phases.

To find the discriminating layers within different datasets, hyperspectral images and products of Airborne Laser Scanning (ALS) statistical analysis were used along with Linear Discriminate Analysis (LDA) and different ANOVA tests. These previously successfully used methods to discriminate vegetation class data and identify the most differentiated

layers within the spectral bands [37,38] or within the vegetation indices [39] for crop identification. Analyses were also used for analysis of different high-Arctic plants [40].

3. Materials and Methods

3.1. Airborne Data Acquisition

The study was based on hyperspectral and ALS data. Three instruments, two HySpex scanners (VNIR-1800 and SWIR-384), and an ALS scanner (Riegl LiteMapper) were placed in the same aircraft and combined as a *HabitARS* platform [41]. The data were acquired simultaneously: hyperspectral images in 451 spectral bands were acquired using a VNIR-1800 (range 400–1000 nm, 182 bands, spectral sampling 3.26 nm, spatial resolution 0.5 m), a SWIR-384 (range 950–2500 nm, 288 bands, spectral sampling 5.45 nm, spatial resolution 1 m), and ALS data acquired with a density of 7 points/m^2 [41]. Overflights were made during three campaigns in 2016: early summer (June 22)—C1, summer (July 24)—C2, and autumn (September 11)—C3. In each of the campaigns, data for the same area were obtained.

A total area of 307 ha was selected for the study, located in the Soła river valley near Oświęcim (southern Poland), where *R. caesius* occurs with high frequency and density (Figure 2). The area was abandoned by agriculture (no treatments, including mowing).

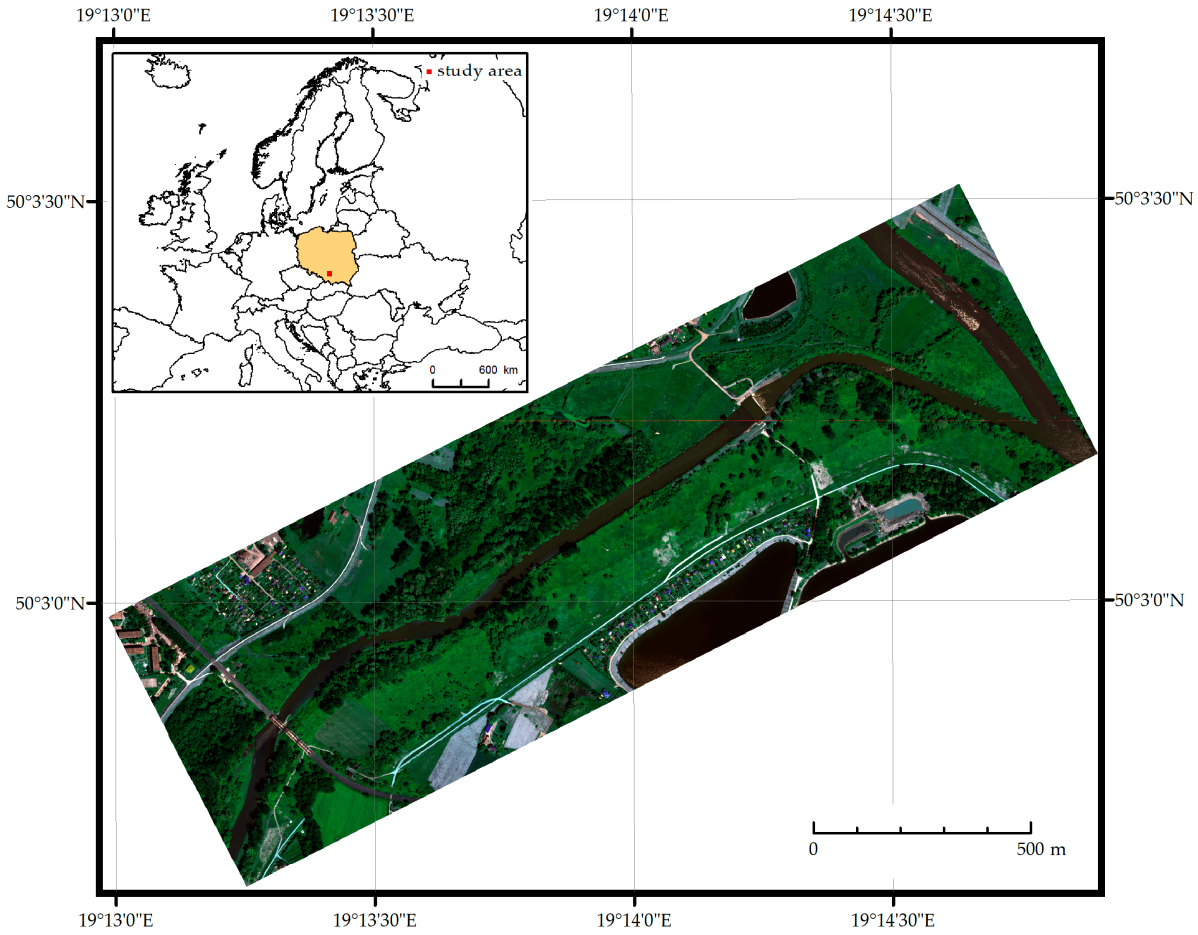

Figure 2. Study area—HySpex image (RGB mosaic) from 22 June 2016 and its location in Europe.

3.2. Acquisition and Preprocessing of Ground Reference Measurements

The field study was done over three campaigns corresponding to the overflights: campaign 1—30–31 May 2016, campaign 2—31 July 2016, campaign 3—21 September 2016. Two types of polygons were established: *Rubus caesius* polygons and other vegetation (non-

Rubus) polygons present in this area. Each *R. caesius* and non-*Rubus* polygon was a circle with a radius of 2 m. The geolocations of the reference polygons were recorded using GNSS Mobile Mapper 120 with real-time differential correction (DGPS) yielding a measurement accuracy from 0.5 to 0.2 m. The polygons were saved in the form of vector shapefiles.

To establish *R. caesius* polygons, during the first campaign, 50 patches in which this species dominated with different percentages of coverage acquired every 10% (from 40 to 100%) were located, and within those patches, reference polygons were established (Figure 3). Each polygon was located within a compact and homogeneous dewberry patch. Species coverage was assessed using the modified Braun–Blanquet method [42] in increments of 10%, where, e.g., 10% means that the coverage of this species was estimated between 5 and 15%. This method is based on field estimation of the percentage coverage of aboveground shoots in the patch and is commonly used in vegetation studies. The information about *R. caesius* coverage in reference was acquired in each campaign.

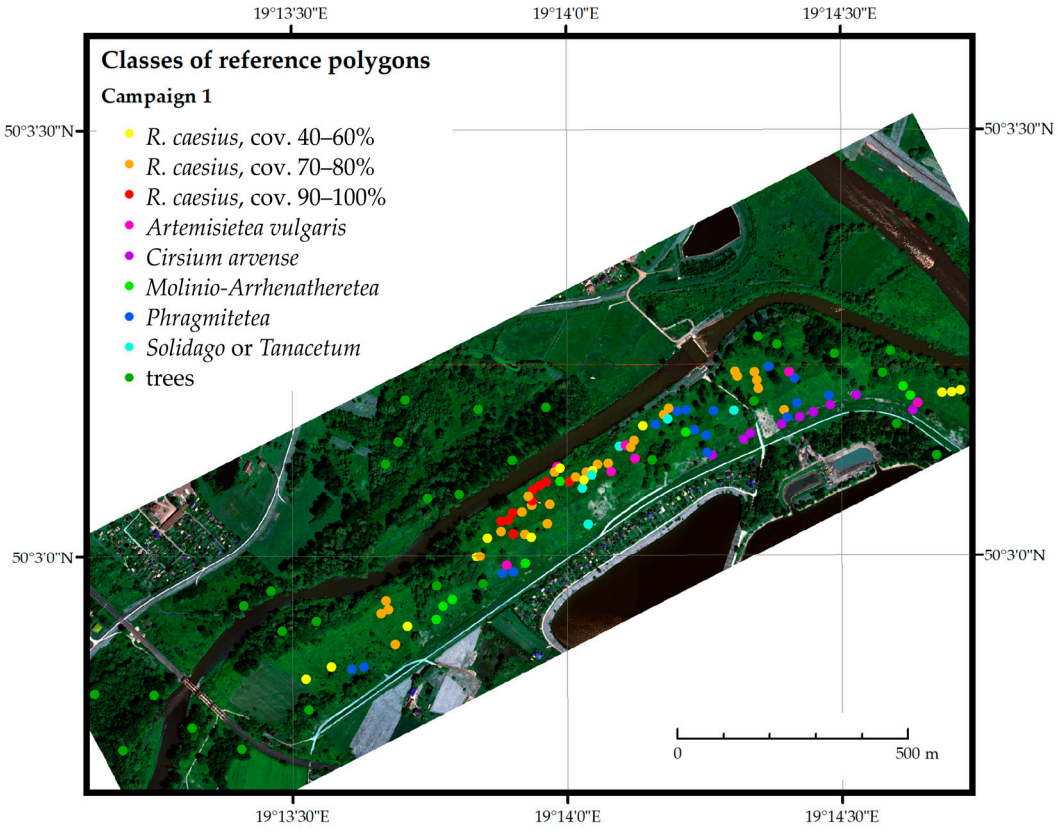

Figure 3. Locations of the reference polygons divided into different classes for the C1 campaign.

Rubus caesius patches varied from single clumps to patches covering several square meters to several dozen square meters. No dry shoots or dry biomass were visible from above in any campaign. An observation chart was created for each of the polygons, which was completed during the second and third campaigns. A summary of *R. caesius*'s developmental phases is included in Table 1.

During the three campaigns, we acquired a total of fifty polygons with vegetation different than *R. caesius*. These polygons covered the entire variability of the surveyed area, including plant communities in which *R. caesius* was recorded or dominated by species with similar morphologies. The following species and types of vegetation were present within the non-Rubus reference plots: *Artemisietea vulgaris*, *Molinio-Arrhenatheretea*, *Phragmitetea* and *Cirsium arvense*, and *Solidago* or *Tanacetum*. The affiliation polygons to the non-*Rubus* subclasses did not change during the vegetation season, so the class obtained once was constant throughout the year (from C1 to C3).

Table 1. The characteristics of *Rubus caesius* and non-*Rubus* vegetation in each campaign.

Field Campaign	Development Phases of *Rubus caesius*	General Characteristics of the Non-*Rubus* Vegetation
C1	Full development of the above-ground parts of the plant: shoots and leaves, up to approximately 50 cm high; leaves mostly herbaceous and bluish; the vegetative phase predominates; in about 30% of the polygons, *R. caesius* plants showed the beginning of flowering	Most of the herbaceous vegetation is similar in height to the *R. caesius* patches; most perennials are in the vegetative stage; some grass species begin flowering
C2	Flowering and fruiting phase; both phases extended over time, not mass-produced flowers or fruits; leaves and shoots herbaceous bluish, glaucous and tinged red where exposed to the sun	Some of the herbaceous plants (*Solidago*, *Phragmites*, *Tanacetum*, *Impatiens glandulifera*, *Artemisia*, *Urtica*) exceed the height of the *R. caesius* patches (1–1.5 m); plants of some species bloom profusely (*Impatiens glandulifera*)
C3	Mostly fruiting phase; fruits not mass-produced, did not stand out from the dominant leaves; leaves and steams herbaceous bluish, glaucous and tinged red where exposed to the sun (more intense process than in C2)	Discolouration of leaves of many species (both herbaceous and woody) appear; visible senescence of spring and early summer species plants (drying out)

All polygons were processed before further analysis. For each campaign, we chose polygons without shadows that had not been mowed or grazed. For each campaign, based on visual interpretation, we also drew 30 polygons for trees.

3.3. Airborne Data Processing

The ALS point cloud orientation was carried out using RiProcess software [43]. The accuracy of this process was assessed at the level of 1 Σsigma = 0.010 cm; then, the data were automatically classified and corrected manually in the TerraSolid software [44]. The classified points were used to generate the Digital Elevation Model (DEM) and Digital Surface Model (DSM) with a 1 m resolution.

The first step in the processing of hyperspectral data was radiometric calibration (performed in the HySpex RAD program, Norsk Elektro Optikk AS, Skedsmokorset, Norway [45]) followed by parametric geometric correction of each pixel (based on ALS' DSM and Inertial Navigation System data) [41]. This process was performed in the PARGE environment (ReSe—Remote Sensing Applications, Wil, Switzerland) [46]. Orthorectification was done using DSM from ALS data. As a result, the pixel location accuracy of RMS = 0.77 m was obtained as compared to orthophotomap with 0.1 m GSD. The atmospheric correction was done in the ATCOR4 program using the MODTRAN5 model (ReSe Applications GmbH, Wil, Switzerland) [47]. The final stage was a mosaic of series made in OrthoVista [48]. Next was the elimination of bands, where the absorption of radiation by water occurs, i.e., 21 bands were removed from the scope of the final scanner due to the range of absorption of radiation by water vapour in the atmosphere (above 2396.44 nm). Finally, an image consisting of 430 bands in the range of 416.18–2396.44 nm was obtained.

To assure the geometrical co-registration, HySpex mosaic and raster derivative products from ALS were integrated into a single set with a standard coordinate system, matrix start point, and pixel size equal to 1 m.

Hyperspectral data were used to calculate 49 remote sensing vegetation indices (VI) in the ENVI 5.3 program using the Spectral Indices function. The list of the indices with the equation is in Table S1.

Based on ALS data, raster layers were created from a point cloud using the *Boise Center Aerospace Laboratory LiDAR* (BCAL) tool [49]. Then, products from the Intensity and Vegetation groups were calculated. The first group of products obtained refers to the intensity of reflectance, while the second refers to the parameters related to the height of the plant cover. The Vegetation Products were calculated based on elevation and the maximum height of canopy (first return of the laser pulses). In addition, from the point

cloud, products related to the vegetation structure were generated in the Orientation and Processing of Airborne Laser Scanning data (OPALS) program [50]. The ALS layers were selected based on their quality: if pixels on vegetation were identified as non-values or a "salt and pepper" effect was visible, the products were not further analysed. The "salt and pepper" effect is the occurrence of noise in the image in the form of isolated pixels with high local spatial heterogeneity between adjacent pixels [51]. We selected four layers from the BCAL Intensity Products: maximum, minimum, mean, and standard deviation. From among the BCAL Vegetation Products, 12 layers related to the height and structure of vegetation cover were used: minimum, maximum, range, mean, and coefficient of variation, alongside seven height percentiles products (the 5th, 10th, 25th, 50th, 75th, 90th, and 95th percentiles of all height points). The OPALS attributes for vegetation were selected, including the normalised mean, median, minimum, maximum, variance, RMS, and quantiles: 0.05, 0.10, 0.25, 0.75, 0.90, and 0.95. For all points, we also chose 4 amplitude parameters: mean, maximum, minimum, and median.

Finally, the following datasets for each campaign were created: hyperspectral bands (HS—430 layers), remote sensing vegetation indices (VI—49 layers), BCAL (4 layers for Intensity and 12 layers for Vegetation), and OPALS (17 layers). All layers were saved with a 1 m resolution corresponding to the HySpex images.

3.4. Statistical Analysis

The next step was an analysis of the differences between *R. caesius* and other types of vegetation based on the calculated remote sensing layers. We also sought to assess the differences between *R. caesius* and other types of vegetation. *Rubus caesius* polygons were divided into three classes for each campaign based on a species percentage coverage of 40–60%, 70–80%, or 90–100% (Table 2). Other classes (non-*Rubus*) were divided based on dominant species (e.g., *Cirsium arvense, Solidago spp.*, and *Tanacetum sp*.) or for polygons without clear one dominant species based on vegetation classes distinguished according to Matuszkiewicz [17] (*Artemisietea, Molinio-Arrhenatheretea, Phragmitetea*).

Table 2. The number of reference polygons acquired during the three field campaigns.

Class of Reference Polygon	C1 (Early Summer)	C2 (Summer)	C3 (Autumn)
R. caesius (coverage 40–60%)	13	1	1
R. caesius (coverage 70–80%)	27	23	24
R. caesius (coverage 90–100%)	9	22	24
Artemisietea vulgaris	7	7	7
Cirsium arvense	9	11	12
Phragmitetea	16	16	16
Molinio-Arrhenatheretea	8	8	8
Solidago or *Tanacetum*	7	8	8
Trees (visual interpretation)	30	30	30
Sum	127	128	131

The above-mentioned round reference vector polygons were rasterised based on remote sensing layers, and pixels that fit entirely within the polygons were used in further analyses. The analyses were performed by comparing classes of *R. caesius* (coverage 40–60%, 70–80%, and 90–100%) to other vegetation classes (non-*Rubus*). In the early summer campaign, three *R. caesius* classes were analysed, whereas in the summer and autumn campaigns, only two were analysed: coverage 70–80% and 90–100% (there were not enough polygons for the *R. caesius* 40–60% class). Based on the number of pixels, six different vegetation classes were chosen for analysis: *Artemisietea vulgaris*, *Molinio-Arrhenatheretea*, *Phragmitetea*, *Cirsium arvense*, *Solidago* with *Tanacetum*, and trees.

To find the most differential layers, a two-stage process was performed for each of the three campaigns. First, all available layers in a given dataset (HS, VI, BCAL, or OPALS) were inspected for a correlation between their bands using a Tau–Kendal test. All layers with a pairwise correlation coefficient higher than 0.95 were removed. Next,

the remaining layers in each dataset were analysed using Linear Discriminant Analysis—LDA [38,40,52]. In the process, forward variable selection for classification using LDA was performed for each analysed dataset. Thus, for each dataset, we were able to rank layers based on their order of selection by LDA and their overall contribution to the correctness rate. The maximum number of layers selected by LDA was limited to 40. During the experiments, none of the datasets had more than 40 layers marked as important. Next, all layers deemed to be important were subject to a Non-Parametric Multivariate Analysis of Variance (NPMANOVA) to determine how good the separation was between classes in the given layers selected by LDA. All analyses were performed in the R software environment [53] using the packages caret [54], klaR [55], and vegan [56].

Different scenarios were analysed, including three *R. caesius* classes dependent on coverage compared to non-*Rubus* classes in three campaigns on four datasets: spectral reflectance (HS), vegetation indices (VI), OPALS, and BCAL. For each of the datasets, 100 iterations of the stratified random sampling procedure were performed, where 30 pixels from the *R. caesius* class and 30 from each of the non-*Rubus* classes were subsampled for decorrelation, LDA layer selection, and NPMANOVA. The pixels were randomised independently of the reference polygons so that each pixel could come from a different polygon or several pixels could be drawn within one polygon. The number of pixels was limited to 30 due to the number of pixels in each class. After analysis, each dataset was characterised by three values: the LDA correctness rate, the NPMANOVA F-value, and the layers that were selected by LDA to be the most useful. Based on the 100 iterations (for each the values of correctness rate, f values, differentiating layers), we identified the most differentiating layers. After 100 iterations of the LDA and NPMANOVA tests the F-values, correctness rates, and useful layer lists were compiled and visualised.

The next step was to analyse the results. Further analyses and interpretations were focused on the best datasets based on the correctness rates and F-values. The values for the BCAL and OPALS layers were noticeably lower compared to the hyperspectral bands and vegetation indices. For 430 spectral bands, the ranges of the spectrum were analysed for each campaign. This study assumed that the wavelength was useful for differentiating three *R. caesius* classes from non-*Rubus* if the band was within 10% of the highest frequency of occurrence. These ranges of the spectrum were analysed.

For the VI dataset, we analysed how many of the 100 iterations of each vegetation index were selected as differentiating. The same applied to HS, for which 10% of the most differentiating bands were analysed. Next, for the selected indices, maps of spatial distribution and values in each campaign were created. Based on this information and botanical knowledge, the data were analysed and interpreted.

4. Results

4.1. Hyperspectral and ALS Data Comparison

The tests indicated the datasets and layers within them that differentiate *R. caesius* classes from non-*Rubus* classes. Based on the correctness rate from LDA and the F-value from NPMANOVA, the values were noticeably lower for the ALS data (the BCAL and OPALS datasets) (Table 3 and Figure 4).

The correctness rate each time for AS products was equal to around 0.857, and there were no differences between iterations and different coverage levels of *R. caesius*. Even though the correctness rate values for ALS were high, this rate was always lower than that for the HS and VI. Based on this information, two datasets, BCAL and OPALS, were excluded from further analysis.

Higher values of the correction rate and F-values and a higher spread were acquired for the hyperspectral data (HS and VI). This differentiation was the greatest for the early-summer campaign (C1), regardless of the coverage class, whereas the smallest was found for the autumn campaign (C3). However, the differences did not exceed a few percent. Higher values were calculated for classes with higher coverage, and the values were also less diverse. The average number of layers used to effectively differentiate the *R. caesius*

class from other vegetation for 100 iterations was similar for all datasets—from 10 to 14. Moreover, for the VI dataset, the F-value was generally higher compared to that of HS.

Table 3. The values of the average correction rate, number of layers defined as differentiating (the result of Linear Discriminate Analysis), and F value (the result of Non-Parametric Multivariate Analysis of Variance) for different datasets and three campaigns (C1, C2, C3) calculated based on 100 iterations.

Scenario	C1			C2		C3	
	cov. 40–60%	cov. 70–80%	cov. 90–100%	cov. 70–80%	cov. 90–100%	cov. 70–80%	cov. 90–100%
Correction rate (based on LDA)							
HS	0.9651	0.9735	0.9830	0.9491	0.9752	0.9083	0.9321
VI	0.9609	0.9816	0.9882	0.9635	0.9808	0.9304	0.9526
OPALS	0.8571	0.8573	0.8572	0.8577	0.8575	0.8573	0.8572
BCAL	0.8571	0.8571	0.8572	0.8573	0.8571	0.8577	0.8581
Number of layers (based on LDA)							
HS	12	11	11	13	17	13	14
VI	12	13	12	11	12	11	11
OPALS	12	12	12	12	13	13	13
BCAL	10	10	10	11	10	11	11
F-value (based on NPMANOVA)							
HS	9.7	10.5	12.0	8.5	9.2	4.7	6.1
C	18.0	16.4	23.5	23.6	42.7	9.7	11.7
OPALS	1.3	1.5	1.1	1.3	1.2	1.0	1.3
BCAL	1.7	1.8	1.5	1.9	2.2	1.1	1.6

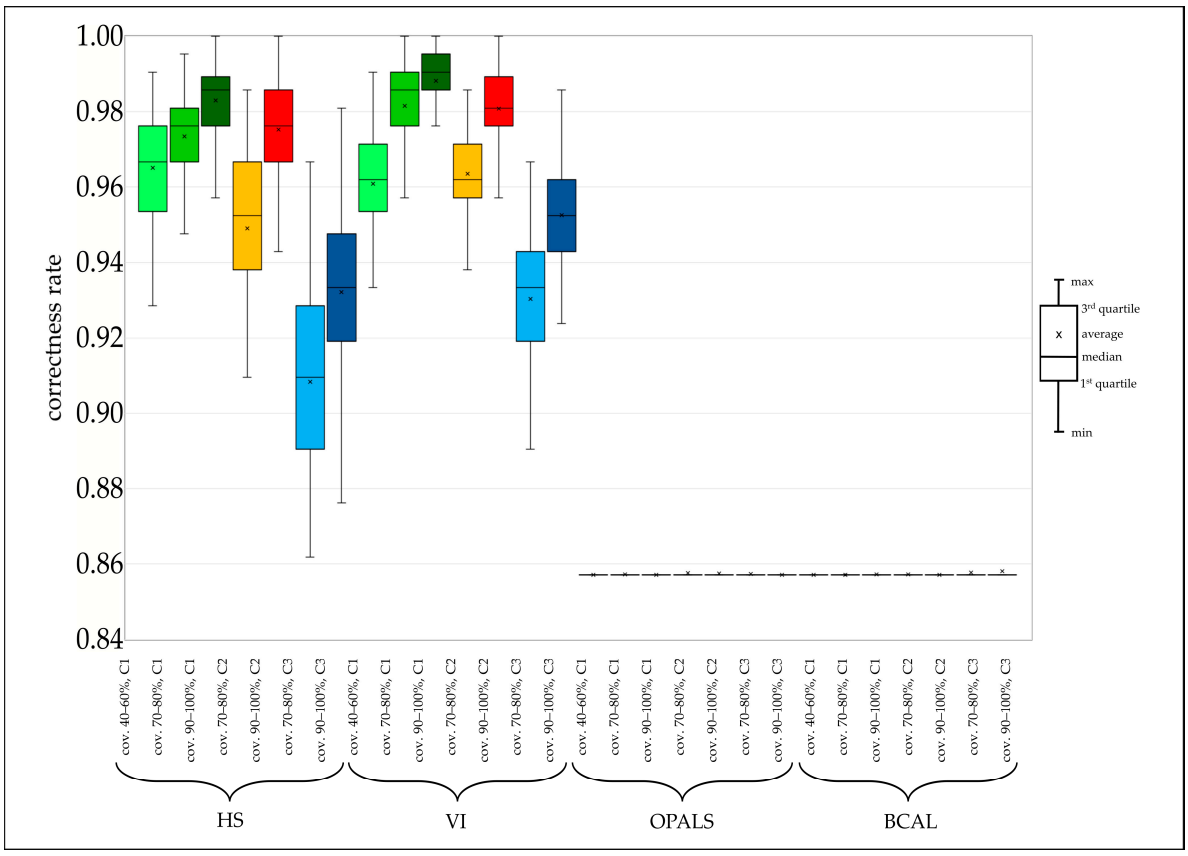

Figure 4. Values of the correctness rate based on 100 iterations for different scenarios.

4.2. Spectral Band Dataset

As a result of the LDA analysis, we determined which spectral bands were the most useful for differentiating *R. caesius* depending on the species coverage and data acquisition date. Considering the spectrum bands with the highest frequency of occurrence as differentiating (10% of all bands), it can be concluded that the spectrum ranges are similar for the three campaigns and varied coverage (Figures 5 and 6).

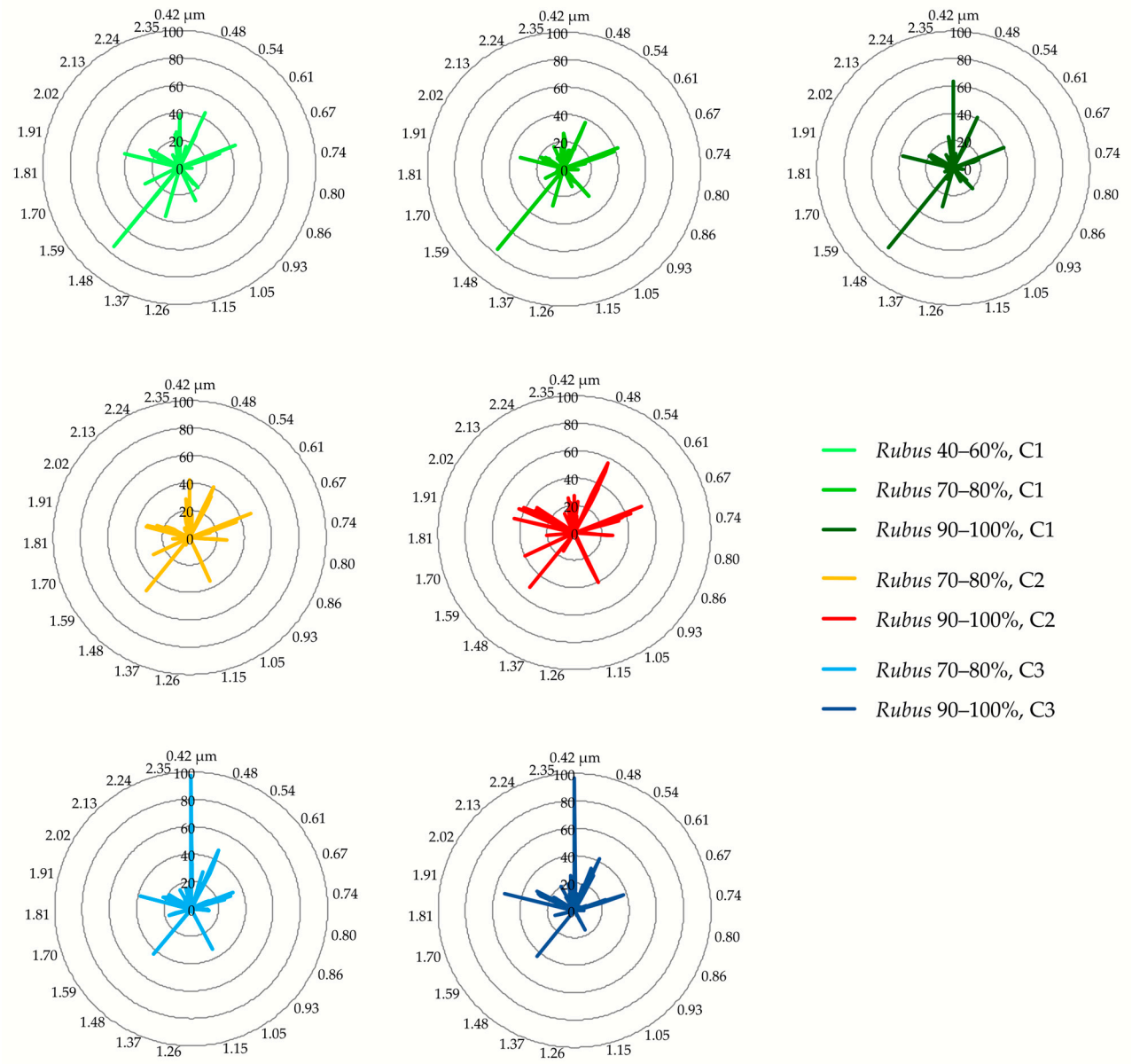

Figure 5. The frequency of the occurrence of each spectral band differentiating varied *Rubus caesius* coverage and campaigns calculated based on 100 iterations of the Linear Discriminate Analysis (LDA) analysis.

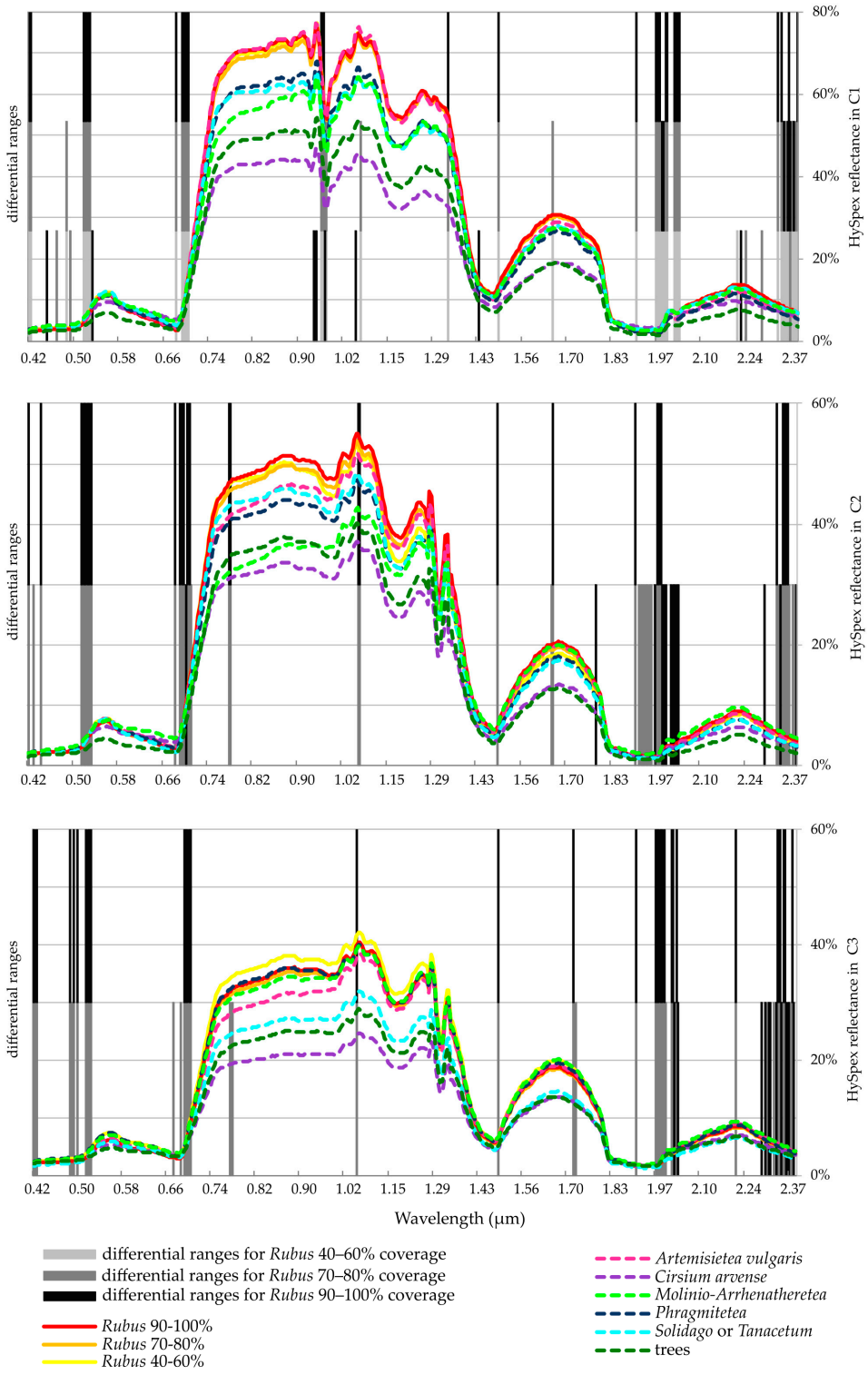

Figure 6. Average spectrum for different classes acquired from HySpex images and the bands (marked in dark grey, medium grey, and light grey dependent on *Rubus* coverage) that were defined as differentiating based on LDA analysis. The spectrum range was defined as differentiating when the frequency of the occurrence was above 15 (10% of 100 iterations).

The differentiating ranges are in VNIR (400–1000 nm) and SWIR (1000–2500 nm). Based on the values of frequency of occurrence, we located bands that were most commonly defined as differentiating in VNIR:

- 416 nm: the first band from blue light, one of the bands with the highest frequency values;
- 515–525 nm: the so-called green edge, where there are absorption bands for carotenoids and partly for chlorophyll;
- 678–707 nm, red-edge: used to determine vegetation conditions;

and in SWIR:

- 1491 nm: a band with the highest frequency of occurrence as differentiating;
- 1908 nm: water absorption bands;
- 1968–2040 nm and bands above 2300 nm: absorption bands for cellulose and lignin.

There were only slight differences between the campaigns. For the early summer campaign (C1, the ranges of 920–970 nm and 1339 nm were used; for the summer campaign (C2), ranges of 774–777 nm were used; and for the autumn campaign (C3), we used 1720 nm, which is the absorption band for cellulose and lignin. For the early summer (C1) and summer (C2) campaigns, SWIR bands around 1665 nm and in the range 1653–1659 nm were observed to differentiate.

4.3. Vegetation Index Dataset

For the VI dataset, we selected the indices that differentiate *R. caesius* classes the most based on the frequency of occurrence in each campaign (Figure 7). There were no significant differences between coverage classes and campaigns. The analysis showed that Normalised Difference Nitrogen Index (NDNI) has the highest potential to differentiate *R. caesius* from other types of vegetation among all analysed indices; in each campaign, at least once, the value of the frequency was above 90. High values were observed for Atmospherically Resistant Vegetation Index (ARVI) and Green Difference Vegetation Index (GDVI), which describe vegetation conditions, and for Cellulose Absorption Index (CAI), which identifies cellulose content. The indices that identify pigment content also had high frequency in each campaign, i.e., Anthocyanin Reflectance Index 1 (ARI1) and Carotenoid Reflectance Index 1 (CRI1).

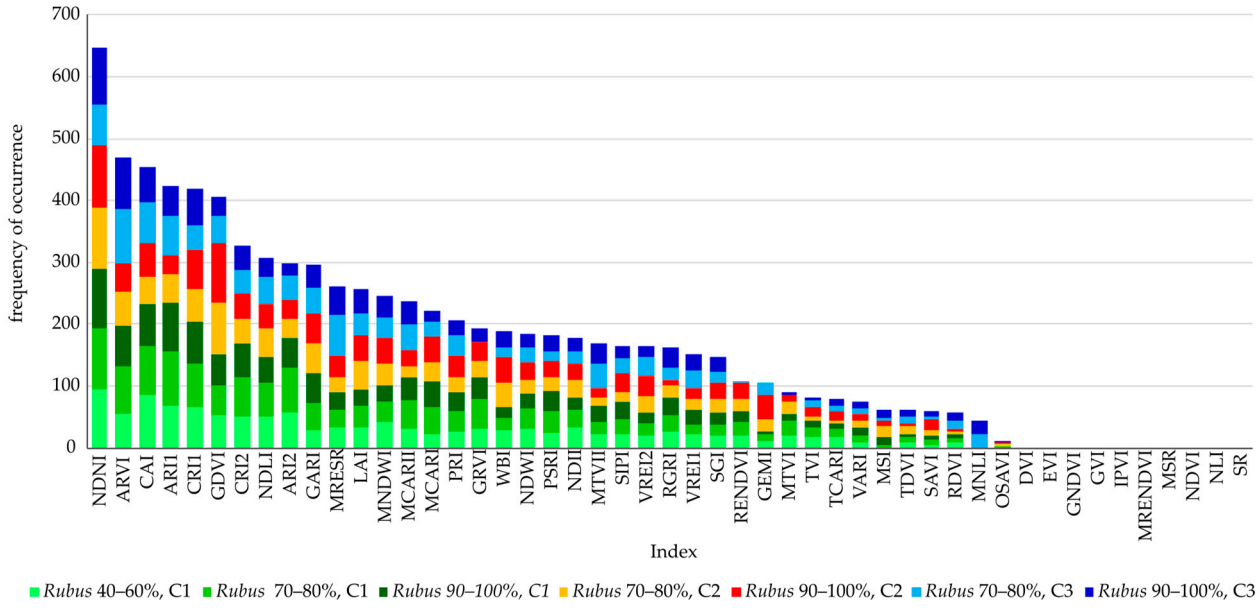

Figure 7. The frequency of the occurrence vegetation indices (VI) as differentiating for varied *Rubus caesius* coverage and campaigns calculated based on 100 iterations of the LDA analysis. Maximum value frequency of occurrence is 700.

When analysing the 10% most frequent vegetation indices in each campaign and *R. caesius* coverage with the highest frequency of occurrence, seven indices were noted: ARI1, CRI1, ARVI, GDVI, CAI, NDNI, and Modified Red Edge Simple Ratio Index (MRESR). However,

the last index was observed only for *R. caesius* coverage of 70–80% for C3 (Table 4). Based on this information, six indices apart from MRESR were chosen for further comparisons (Figure 8).

Table 4. Vegetation indices (with information about spectrum used to calculate them) listed and marked with "+" among the 10% most differentiating layers for each campaign (C1, C2, C3) and specified *Rubus caesius* coverage.

VI	Spectrum Used for Calculation in nm	C1			C2		C3	
		cov. 40–60%	cov. 70–80%	cov. 90–100%	cov. 70–80%	cov. 90–100%	cov. 70–80%	cov. 90–100%
ARI1	550, 700	+	+	+				
ARVI	BLUE, RED, NIR		+	+	+		+	+
CAI	1680, 1754	+	+	+		+	+	+
CRI1	510, 550	+		+	+	+		+
GDVI	RED, NIR				+	+		
MRESR	445, 705						+	
NDNI	1510, 1680	+	+	+	+	+	+	+

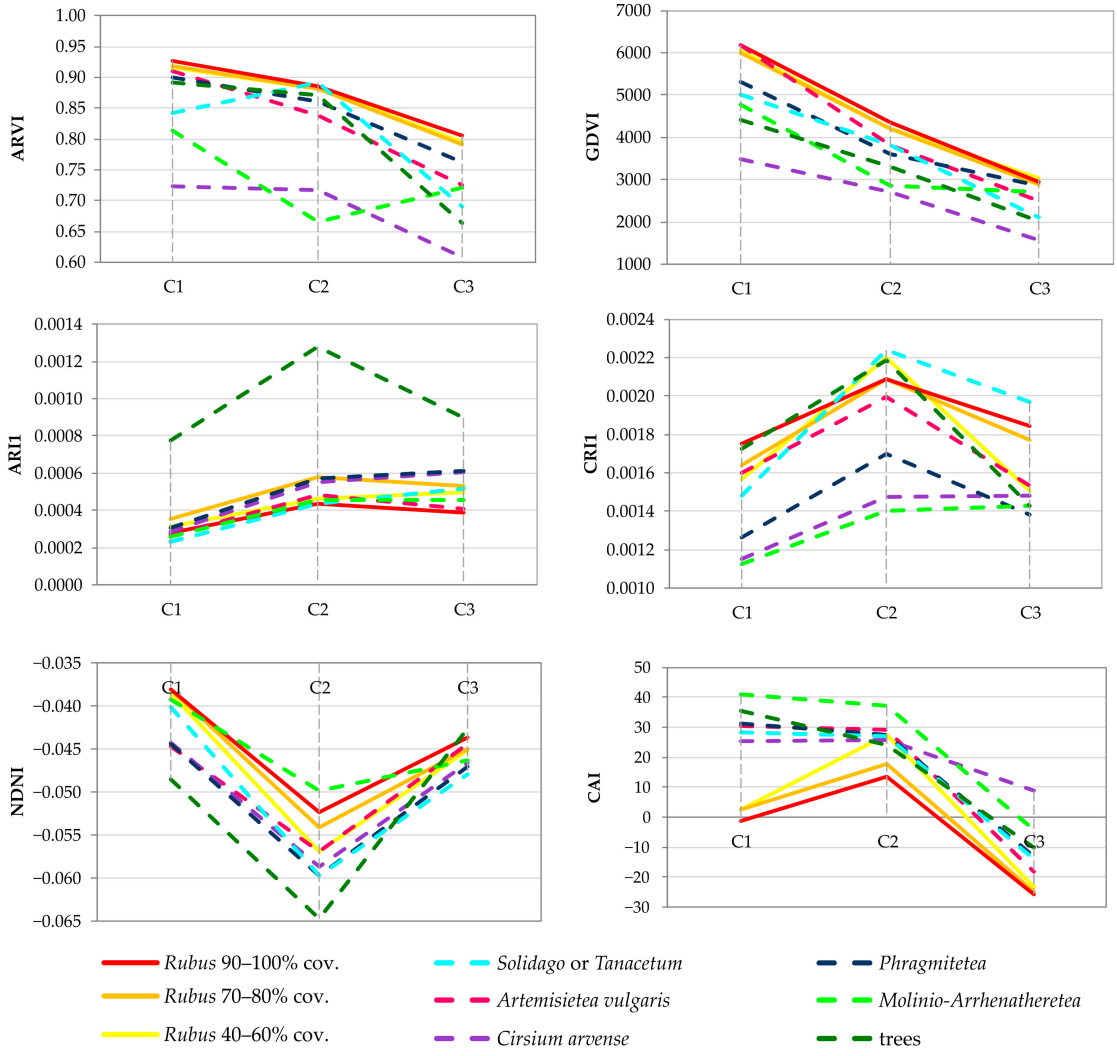

Figure 8. The average values of the selected vegetation indices for the analysed *R. caesius* and other vegetation classes for the three campaigns.

The information on vegetation conditions was based on two analysed indices, ARVI and GDVI, which showed similar tendencies (Figures 8 and 9). The ARVI for *R. caesius* and most other tested types of vegetation had the highest values in early summer (C1); the average for all classes was 0.87, and the lowest in autumn (C3) was 0.73. Regardless of the examined term, the ARVI reached higher values for *R. caesius* (regardless of the percentage coverage) compared to other types of vegetation (except for patches with *Solidago* with *Tanacetum*) in C2. Within individual campaigns, the plots with varied *R. caesius* percentages differed only by 0.01. The GDVIs for *R. caesius* and for other types of vegetation were maximum in early summer (C1) and minimum in autumn (C3) (Figure 8 and Figure S2). The range of variation of this index for *R. caesius* during the growing season was 3308 points, from 6187 in C1 to 2879 in C3. Importantly, this index reached, on average, higher values for *R. caesius* (regardless of coverage) than for other types of vegetation. Only in early summer was the GDVI value for the vegetation of *Artemisietea vulgaris* class similar to that of *R. caesius*, while in autumn, only the value for rushes (*Phragmitetea*) was similar. The GDVI values for the three *R. caesius* coverage classes showed the same tendencies and slight differentiation within the campaign (maximum 190 points for C1).

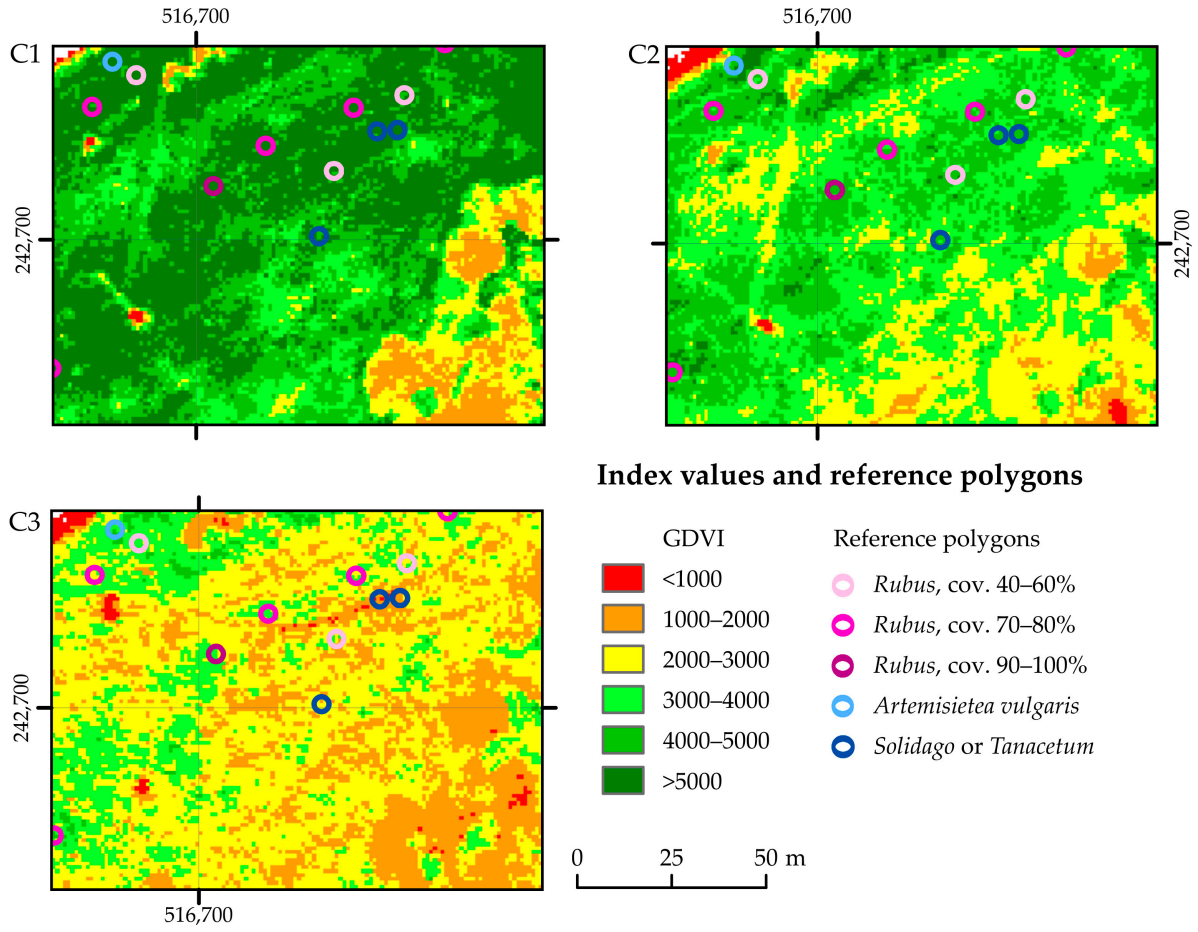

Figure 9. The spatial distribution of the Green Difference Vegetation Index (GDVI) classes for the three campaigns in the selected area.

The indices related to pigment content generally had the highest values in summer. The ARI1 for the *R. caesius* class described the highest values in summer (C2), with 0.000579 at 70–80% coverage, and the lowest values in early summer, with 0.000314 for 40–60% coverage (Figure 8 and Figure S1). In each of the three campaigns, we observed the highest values of the index for coverage of 70–80%. In early summer, for the *R. caesius* classes, this index had slightly higher values than those of non-*Rubus* types of vegetation. In

summer and autumn (C2 and C3), the values were different in relation to the other types of non-forest vegetation, but differences were also observed for the three *R. caesius* classes. Only trees were characterised by a significantly higher value of ARI1. The CRI1 had the highest values for the *R. caesius* class in summer (C2), with 0.0022, and the lowest values in autumn (C3), with 0.0015 (Figure 8 and Figure S4). For all tested types of vegetation, this index provided maximum values in summer. There was also a significantly greater variability of the index for the coverage class of 40–60% *R. caesius* than for higher coverage classes. In autumn, this species with a coverage of 70 to 100% was distinguished by a significantly higher value of CRI1 than most other types of examined non-forest vegetation. Only patches with *Solidago* and/or *Tanacetum* reached higher values in C3.

The values of NDNI, which shows the nitrogen content, were characterised by low variability within and between campaigns and presented values below 0 (Figure 8 and Figure S5). The values of this index ranged from −0.0381 for *R. caesius* in campaign C1 to –0.0647 for trees during campaign C2 (summer). The lowest value of this index was found in summer (C2). The highest values, depending on the type of vegetation, were found in early summer or autumn. The biggest differences between *Rubus caesius* and other vegetation classes were found in the summer campaign. For *R. caesius*, with coverage of 70–100%, the values were the highest apart from *Molinio-Arrhenatheretea*.

The cellulose content based on CAI, regardless of the campaign, was, on average, lower for *R. caesius* than for other types of vegetation (Figure 8 and Figure S4). The values of this index were the lowest in autumn (C3), with an average 14 points, and the highest in summer (C2), with an average of 25 points. The difference between the values for *R. caesius* and other types of vegetation was the highest in early summer (C1). The value of the CAI index decreased with *R. caesius* coverage in each pixel.

5. Discussion

5.1. Remote Sensing Data that Differentiate Rubus Caesius from Its Background

The performed analysis demonstrated that HS data and their products are useful for differentiating *R. caesius* from other vegetation types, whereas the results for ALS data were good but less useful in this application (Table 3 and Figure 4). Based on spectral information, it is possible to describe the biophysical components of the plants; the composition differs between species, so it is possible to use this kind of data for plant phenotyping [57]. *Rubus* is an expansive species that has different values for its biophysical variables (e.g., pigment content) and different vegetation condition (phenology) compared to other vegetation. This is why the VI, which indicates the status of the plants, differentiated *R. caesius* from non-*Rubus* vegetation.

The results of the LDA and NPMANOVA tests indicate that it is possible to differentiate the classes based on ALS products into BCAL and OPALS, but it is much more effective to use the HS bands or VI. Similar conclusions were obtained for *Spiraea tomentosa* mapping using ALS and hyperspectral data [58]. The ALS data were used to model the 3D construction of the vegetation canopy. *Rubus caesius* is surrounded by vegetation with a similar structure, so differentiation between species is possible only to a certain extent on the basis of parameters such as vegetation height and related derivatives. In this study, ALS data were used with a density of 7 points/m^2, and all products were calculated with a 1-m spatial resolution. Using a higher point density or changing other ALS parameters could be useful for acquiring more detailed information. Moreover, different ALS products could be more successful than those used in this study. The ALS products were used for *Rubus* identification combined with HS data [32–34]. ALS data have rarely been used for the classification of non-forest vegetation. Based on ALS derivatives, were classified 24 types of vegetation in the Natura 2000 habitats, including salt marshes and steppic grasslands [59,60]. In the analyses, we used 18 variables from an ALS acquired in the growing season and three variables based on a DTM acquired in the leaf-off season. One of the key factors of effective differentiation was height. At the same time, hyperspectral data and ALS products were tested for detecting *Spiraea tomentosa* [58]. Using only the ALS

product classification resulted in low accuracy (F1 for the *S. tomentosa* equalled about 42% depending on the time of data acquisition), while using only Minimum Noise Fraction bands, the value of F1 was at least 77%. A combination of these data resulted in a lower accuracy than that based only on the MNF bands (F1 about 68%).

In summary, for *Rubus* differentiation, ALS parameters are less useful compared to optical data probably because the height of *Rubus* is similar to that of the surrounding vegetation. However, based on the previous research, it can be stated that the combination of the two types of data increases the accuracy of the classification. Data fusion was tested for *R. caesius* classification [31] as well as for different types of vegetation [61–63]. At the same time, the combination of hyperspectral and ALS data was not tested in this study. The use of different types of data generally increases the cost and time of classification, which makes the monitoring more difficult.

The differentiation results in this study were slightly better for early summer and became worse with the flowing growing season. However, the differences were not significant, so it can be assumed that it is possible to distinguish *Rubus* from other species during most of the growing season. The previous results indicated summer to be the best time for data acquisition [35]. The classification of *Rubus cuneifolius* was performed in four seasons based on Landsat 8 and Sentinel-2 data. The obtained accuracies were not high, but there were some differences between the campaigns; the best results were acquired in the summer, and the worst were obtained in the winter.

5.2. Relation between Remote Sensing Data and the Functional Traits of Rubus Caesius

Based on the performed analysis, the results were found to be repetitive in each campaign—the generally determined VIs were based on the spectrum ranges defined as differentiating. There were slight shifts in the spectrum between campaigns, but most of the significant bands were similar. The shifts may be due to changes in incoming radiation or, less likely, to imperfections in the atmospheric correction. Two out of the seven most differentiating indices, ARVI and GDVI (Figure 8), used wide spectral ranges in the visible (red and blue) and near infrared spectra and were also indicated as discriminating based on LDA (Figure 6). The wavelengths that were used to calculate the VI of the pigment content (ARI1—700 nm and CRI1—510 nm) and used in the CAI (2000, 2200 nm) and NDNI (1510, 680 nm) indices were partially defined as differentiating.

Differences were observed between the conclusions from the HS and VI datasets for ranges of 1968–2040 nm and bands above 2300 nm. The water content indices were not highlighted as the most differentiated indices. Water absorption bands are located in this spectrum range, so this range may be important for differentiating *R. caesius* from non-*Rubus*; however, these bands also had more noise than others.

A comparison between the three campaigns highlighted the potential weaknesses of the method. For the early summer campaign (C1), the significant ranges were around 960 nm. At the same time, these bands had significant noise due to errors in data acquisition, which is visible in the spectral profile (Figure 6). The errors are probably related to the gap in spectrum during image acquisition and therefore, difficulty in combining data from two scanners (HySpex VNIR-1800 and SWIR-384). It can be concluded that in the case of acquisition errors, such a range could be incorrectly indicated as differentiating.

Based on the acquired results, it can be stated that four out of the seven most differentiating VIs had indicative values for *R. caesius* during the whole vegetation period: ARVI, CAI, CRI1, and NDNI (Table 4). The other three were only indicative in individual campaigns, with ARI1 in early summer (C1), GDVI in summer (C2), and MRESR in autumn (C3).

The highest information potential was presented by the NDNI, which assumes average higher values for *R. caesius* than for the non-*Rubus* vegetation throughout the growing season (Figure 8). The NDNI shows the nitrogen content in the leaves, which was proven for species growing in natural ecosystems such as the common reed (*Phragmites australis*) [64] and crops [65]. The large separability potential for the NDNI is likely due to the fact that

R. caesius is a nitrophilous species [66] and may have a higher nitrogen content in its leaves than non-*Rubus* species. The maximum average NDNI value was additionally observed in early summer when, according to the results of the previous research, *Rubus* has the highest nitrogen content in tissues [67].

Another VI with a high separability potential is ARVI, which describes the plant's condition when reducing the influence of the atmosphere. This VI was used, among others, to identify *Xylella fastidiosa* infection in olive orchards [68]. On average, reference polygons with *R. caesius* have higher values of ARVI then non-*Rubus* species throughout the growing season and decrease from C1 to C3. High values of this VI are associated with high chlorophyll content in dewberry leaves [69]. CAI also has a high potential to identify *Rubus*, with average values significantly lower for *Rubus* than for the background (Figure 8). This lower value is related to the biology of the investigated species, where the CAI value is strongly related to the presence/visibility of the non-photosynthetic parts of plants [70], litter/dry biomass [69], and senesced vegetation [71]. The non-*Rubus* class consists mainly of non-forest communities constructed with perennials or annual species characterised by a relatively large coverage of dry biomass. On the other hand, the patches with *R. caesius* are characterised by high vigour and large coverage with horizontally oriented photosynthetic leaves. This was also confirmed by the high GDVI values compared to the background, which indicated a correlation with the Leaf Area Index [72]. Another important factor for distinguishing *R. caesius* from the background is the pigment indices such as CRI1, which describes the carotenoid content in plant tissues. The values of the CRI1 indicate that *R. caesius* is also characterised by a higher content of carotenoids compared to non-*Rubus* vegetation, which is related to the presence of high chlorophyll content, mainly to protect the photosynthetic system against photooxidation [69]. High carotenoid content is particularly visible in summer (C2) and autumn (C3) (Figure 8) for leaves exposed to full sun.

5.3. Remote Sensing Data Useful for Rubus Caesius Identification

Considering the aforementioned information, it can be assumed that the use of data with high spectral resolution is unnecessary because it is possible to detect *R. caesius* using only a few spectral ranges—much wider than those used in HS data. Based on the acquired results, it is possible to determine which ranges and bands allow one to differentiate *R. caesius* from non-*Rubus*. Considering the possibility of calculating the VI (ARVI and GDVI), it is important to use data in the visible and near infrared range. A red-edge band and potentially the water absorption range would also be useful.

Most of the previous studies on genus *Rubus* mapping were based on HS data. The following species were analysed with these data: *R. armeniacus*, *R. fruticosus*, and *R. caesius* [30–34]. This identification was mostly successful but also time consuming. It was possible to classify *R. fruticosus L.* agg. using HyMap [30] and *Rubus spp.* using HySpex [31]. Further, *Rubus armeniacus* was identified based on CASI and ALS products [32–34]. Again, these approaches were successful but also time-consuming, so their use in monitoring would likely be ineffective. Good results were acquired for *Rubus cuneifolius* (the best results among all tested methods were an OA of 82% and a kappa of 0.71) based on SPOT 5 [36]. In this research, the authors also suggested that successful mapping of the species is dependent, e.g., on the spatial and spectral resolution, patch size, time of acquisition, and other vegetation in the background.

An example of a sensor based on the aforementioned conditions that is not suitable for *R. cuneifolius* identification and has already been tested is Landsat (PA 52% and UA 45% for the best classification) [35]. The authors concluded that the images' spatial resolution was insufficient but also that the red-edge is not missing.

An example of a sensor that meets the aforementioned conditions is Sentinel-2, which offers a sufficient spectral resolution. The sensor also has red-edge and short-wave infrared bands. The spatial resolution makes it possible to identify *R. caesius* patches. The temporal resolution is also sufficient to acquire cloudless images during the whole growing season,

including summer. Moreover, these data can be used for easy vegetation monitoring, as they are provided free of charge. Using this sensor, *R. cuneifolius* was classified with a PA of 80% and a UA of 45% [35]. The authors proved that the Sentinel-2 bands of NIR, red-edge, and SWIR are crucial in mapping, which is also a conclusion in the present study. Higher accuracy could possibly be achieved by using vegetation indices calculated based on Sentinel-2. However, the resolution of the Sentinel-2 data may be a limitation to its use. In case of dominance of small patches (below 20 m^2) linear spectral unmixing might be necessary to identify the *Rubus*. WorldView-3 could be a useful sensor for identification with a higher spatial resolution and at the same time potentially sufficient spectral resolution. It was already successfully used to with GEOBIA to extract olive tree crowns [73], oil palms [74], or broadleaf trees [75].

6. Conclusions

Based on the performed analysis, *Rubus caesius* can be distinguished from the background using optical data. Differentiation based on LDA and NPMANOVA analyses were successful for each of the analysed campaigns in early summer, summer, and autumn. ALS data were less useful for identification, which may be related to the insufficient variation between *Rubus* and non-*Rubus* classes in vegetation height.

Differentiation was possible for each *R. caesius* coverage class (40–60%, 70–80%, and 90–100%), but higher values of the correctness rate were observed for coverage of 90–100%. It was proven that regardless of the time of image acquisition, the selected spectral ranges were sufficient to differentiate *R. caesius* from non-*Rubus*. The analysis indicated what spectral ranges can be useful: visible (especially blue and red light), red-edge, near infrared, and possibly SWIR ranges are essential. It was proven that certain vegetation indices can differentiate *R. caesius* from other species, including ARI1, CRI1, ARVI, GDVI, CAI, NDNI, and MRESR. Only NDNI differentiated species regardless of the acquisition date and *R. caesius* coverage, while the other indices were not useful for every analysed scenario. For example, ARI1 could be used in early summer, and GDVI could be used in summer. The VI values were also found to be consistent with *Rubus*' biophysical properties. On this basis, it can be concluded that the selected variables were not random and can be used in classifications for different areas and times.

The obtained results indicate that it is possible to classify *R. caesius* using images with a lower spectral resolution than HS data. The high spectral and radiometric resolution makes it possible to identify brambles with high accuracy, but a great deal of information must be processed using dedicated algorithms, which takes considerable time. At the same time, identification of the species in monitoring must be precise and as fast and easy as possible. Moreover, the procedure should be repeatable in different areas and as simple as possible to carry out. Monitoring protected vegetation areas requires easy species identification, especially identification of species that pose a threat to natural habitats and valuable plant species. The spatial extent of *R. caesius* as an expansive species, should be monitored, as it poses a serious threat to biodiversity.

There is a need for interdisciplinary collaborations between ecologists and RS specialists to develop new methods for studying invasion [76]. Combining remote sensing technology with botanical knowledge will help us understand the interactions between radiation and vegetation and to map functional traits. This will enable information to be scaled over large areas.

The next steps for researching *Rubus caesius* mapping should be performed based on multispectral images, which is consistent with the specified assumptions. It should also be tested whether these data will be useful in other areas, with different sizes of patches, or for other *Rubus* species.

Supplementary Materials: The following are available online at https://www.mdpi.com/2072-4292/13/1/107/s1, Table S1: Remote sensing vegetation indices used in the study. R—reflectance value; Figure S1: The spatial distribution of ARI2 classes for three campaigns in the selected area; Figure S2: The spatial distribution of ARVI classes for three campaigns in the selected area; Figure S3: The spatial distribution of CAI classes for three campaigns in the selected area; Figure S4: The spatial distribution of CRI1 classes for three campaigns in the selected area; Figure S5: The spatial distribution of NDNI classes for three campaigns in the selected area.

Author Contributions: Conceptualisation, A.J.; formal analysis, A.J., D.K., and E.R.; investigation, A.J., D.K., and E.R.; methodology, A.J., D.K., and E.R.; resources, A.J., D.K., and B.T.-G.; software, D.K.; Supervision, A.J., and B.T.-G.; validation, A.J., D.K., and B.T.-G.; visualisation, A.J.; writing—original draft, A.J., D.K., and E.R.; writing—review and editing, B.T.-G. All authors have read and agreed to the published version of the manuscript.

Funding: This research was funded by the Polish National Centre for Research and Development (NCBR) under the programme "Natural Environment, Agriculture and Forestry" BIOSTRATEG II.: The innovative approach supporting monitoring of non-forest Natura 2000 habitats, using remote sensing methods (HabitARS), grant number: DZP/BIOSTRATEG-II/390/2015 (the Consortium Leader is MGGP Aero. The project partners include the University of Lodz, the University of Warsaw, Warsaw University of Life Sciences, the Institute of Technology and Life Sciences, the University of Silesia in Katowice, and Warsaw University of Technology) and UW Excellence Initiative - Research University. Grant num. BOB-661-463-2020".

Institutional Review Board Statement: Not applicable.

Informed Consent Statement: Not applicable.

Data Availability Statement: The data presented in this study are available on request from the corresponding author. The data are not publicly available due to restrictions of founding institution NCBR.

Acknowledgments: The authors would like to thank the whole Consortium for their work in the HabitARS project, especially the project manager, Łukasz Sławik, from MGGP Aero; the University of Silesia researchers for botanical data acquisition, Andrzej Pasierbiński and Barbara Fojcik; Bogdan Zagajewski and Anita Sabat-Tomala from the University of Warsaw for spectrum collection for atmospheric correction; and Jan Niedzielko and Jaromir Borzuchowski from MGGP Aero company for data processing management. We are also grateful to reviewers who allowed us to improve the manuscript.

Conflicts of Interest: The authors declare no conflict of interest.

References

1. Hooper, D.U.; Chapin, F.S.; Ewel, J.J.; Hector, A.; Inchausti, P.; Lavorel, S.; Lawton, J.H.; Lodge, D.M.; Loreau, M.; Naeem, S.; et al. Effects of Biodiversity on Ecosystem Functioning: A Consensus of Current Knowledge. *Ecol. Monogr.* **2005**, *75*, 3–35. [CrossRef]
2. Hejda, M.; Pyšek, P.; Jarošík, V. Impact of Invasive Plants on the Species Richness, Diversity and Composition of Invaded Communities. *J. Ecol.* **2009**, *97*, 393–403. [CrossRef]
3. Van der Putten, W.H. Climate Change, Aboveground-Belowground Interactions, and Species' Range Shifts. *Annu. Rev. Ecol. Evol. Syst.* **2012**, *43*, 365–383. [CrossRef]
4. Bellard, C.; Thuiller, W.; Leroy, B.; Genovesi, P.; Bakkenes, M.; Courchamp, F. Will Climate Change Promote Future Invasions? *Glob. Chang. Biol.* **2013**, *19*, 3740–3748. [CrossRef]
5. Early, R.; Bradley, B.A.; Dukes, J.S.; Lawler, J.J.; Olden, J.D.; Blumenthal, D.M.; Gonzalez, P.; Grosholz, E.D.; Ibañez, I.; Miller, L.P.; et al. Global Threats from Invasive Alien Species in the Twenty-First Century and National Response Capacities. *Nat. Commun.* **2016**, *7*, 12485. [CrossRef]
6. Marrs, R.H.; Kirby, K.J.; Le Duc, M.G.; McAllister, H.; Smart, S.M.; Oksanen, J.; Bunce, R.G.H.; Corney, P.M. Native Dominants in British Woodland—A Potential Cause of Reduced Species-Richness? *New J. Bot.* **2013**, *3*, 156–168. [CrossRef]
7. Essl, F.; Bacher, S.; Genovesi, P.; Hulme, P.E.; Jeschke, J.M.; Katsanevakis, S.; Kowarik, I.; Kühn, I.; Pyšek, P.; Rabitsch, W.; et al. Which Taxa Are Alien? Criteria, Applications, and Uncertainties. *BioScience* **2018**, *68*, 496–509. [CrossRef]
8. Hejda, M.; Štajerová, K.; Pergl, J.; Pyšek, P. Impacts of Dominant Plant Species on Trait Composition of Communities: Comparison between the Native and Invaded Ranges. *Ecosphere* **2019**, *10*. [CrossRef]
9. Vitousek, P.M. Biological Invasions as Global Environmental Change. *Am. Sci.* **1996**, *84*, 468–478.
10. Williams, D.G.; Baruch, Z. African Grass Invasion in the Americas: Ecosystem Consequences and the Role of Ecophysiology. *Biol. Invasions* **2000**, *2*, 123–140. [CrossRef]

11. Sakai, A.K.; Allendorf, F.W.; Holt, J.S.; Lodge, D.M.; Molofsky, J.; With, K.A.; Baughman, S.; Cabin, R.J.; Cohen, J.E.; Ellstrand, N.C.; et al. The Population Biology of Invasive Species. *Annu. Rev. Ecol. Syst.* **2001**, *32*, 305–332. [CrossRef]
12. Hillebrand, H.; Bennett, D.M.; Cadotte, M.W. Consequences of Dominance: A Review of Evenness Effects on Local and Regional Ecosystem Processes. *Ecology* **2008**, *89*, 1510–1520. [CrossRef] [PubMed]
13. Alice, L.A.; Campbell, C.S. Phylogeny of Rubus (Rosaceae) Based on Nuclear Ribosomal DNA Internal Transcribed Spacer Region Sequences. *Am. J. Bot.* **1999**, *86*, 81–97. [CrossRef] [PubMed]
14. The Plant List. Version 1.1. Available online: http://www.theplantlist.org/ (accessed on 10 May 2020).
15. Zielinski, J.; Kosiński, P.; Tomaszewski, D. The Genus Rubus (Rosaceae) in Southeastern Lower Silesia (Poland). *Pol. Bot. J.* **2004**, *49*, 161–180.
16. Oklejewicz, K. Distribution Patterns of Rubus Species (Rosaceae) in the Eastern Part of the Polish Carpathians. *Pol. Bot. Stud.* **2006**, *21*, 1–98.
17. Matuszkiewicz, W. *Przewodnik do Oznaczania Zbiorowisk Roślinnych Polski*; Wydawnictwo Naukowe PWN: Warsaw, Poland, 2011.
18. Bâbuţ, C.; Manea, D. Controlling the Perennial Species Rubus Caesius L.—A Problem Weed in Winter Wheat and Grain Maize in Tioişoara Area. *Res. J. Agric. Sci.* **2010**, *42*, 8–14.
19. Bâbuţ, C.; Manea, D. Chemical Control Startegies of Rubus Caesius L. in Grain Maize. *Res. J. Agric. Sci.* **2010**, *42*, 3–7.
20. Edees, E.S.; Newton, A.; Kent, D.H. *Brambles of the British Isles*; Ray Society: London, UK, 1988.
21. Wielgosz, T. *Wielka Księga Ziół Polskich*; Elipsa: Poznań, Poland, 2008.
22. Dudzinska, D.; Bednarska, K.; Boncler, M.; Luzak, B.; Watala, C. The Influence of Rubus Idaeus and Rubus Caesius Leaf Extracts on Platelet Aggregation in Whole Blood. Cross-Talk of Platelets and Neutrophils. *Platelets* **2016**, *27*, 433–439. [CrossRef]
23. Grochowski, D.M.; Paduch, R.; Wiater, A.; Dudek, A.; Pleszczyńska, M.; Tomczykowa, M.; Granica, S.; Polak, P.; Tomczyk, M. In Vitro Antiproliferative and Antioxidant Effects of Extracts from Rubus Caesius Leaves and Their Quality Evaluation. *Evid. Based Complement. Alternat. Med.* **2016**, *2016*, 5698685. [CrossRef]
24. Widrlechner, M.P.; Wagner, W.H. Occurrence of European Dewberry, Rubus Caesius (Rosaceae), Naturalized in Iowa and Michigan. *Mich. Bot.* **1998**, *37*, 107–112.
25. Mróz, W.; Baba, W. *Monitoring of Natural Habitats. Methodological Guide for Natural Habitat 6210 Xerothermic Grasslands (Festuco-Brometea)*; Library of Environmental Monitoring; Inspection of Environmental Protection: Warsaw, Poland, 2017; pp. 1–14.
26. Korzeniak, J. *Monitoring of Natural Habitats. Methodological Guide for Natural Habitat 6520 Mountain Yellow Trisetum and Bent-Grass Hay Meadows (Polygono Trisetion and Arrhenatherion)*; Library of Environmental Monitoring; Inspection of Environmental Protection: Warsaw, Poland, 2017; pp. 1–17.
27. Korzeniak, J. Ekstensywnie Użytkowane Niżowe Łąki Świeże (Arrhenatherion). In *Monitoring Siedlisk Przyrodniczych. Przewodnik Metodyczny Część Trzecia*; Library of Environmental Monitoring; Inspection of Environmental Protection: Warsaw, Poland, 2012; pp. 79–94.
28. Pawlaczyk, P. *Methodology of Nature Monitoring. Methodological Guide for: Natural Habitats: 4030 Dry Heath Communities Calluno-Genistion, Pohlio-Callunion, Calluno-Arctostaphylion*; Library of Environmental Monitoring; Inspection of Environmental Protection: Warsaw, Poland, 2017; pp. 1–19.
29. Perzanowska, J.; Korzeniak, J.; Chmura, D. Alien Species as a Potential Threat for Natura 2000 Habitats: A National Survey. *PeerJ* **2019**, *7*, e8032. [CrossRef] [PubMed]
30. Dehaan, R.; Louis, J.; Wilson, A.; Hall, A.; Rumbachs, R. Discrimination of Blackberry (Rubus Fruticosus Sp. Agg.) Using Hyperspectral Imagery in Kosciuszko National Park, NSW, Australia. *ISPRS J. Photogramm. Remote Sens.* **2007**, *62*, 13–24. [CrossRef]
31. Sabat-Tomala, A.; Raczko, E.; Zagajewski, B. Comparison of Support Vector Machine and Random Forest Algorithms for Invasive and Expansive Species Classification Using Airborne Hyperspectral Data. *Remote Sens.* **2020**, *12*, 516. [CrossRef]
32. Chance, C.M.; Coops, N.C.; Crosby, K.; Aven, N. Spectral Wavelength Selection and Detection of Two Invasive Plant Species in an Urban Area. *Can. J. Remote Sens.* **2016**, *42*, 27–40. [CrossRef]
33. Chance, C.M.; Coops, N.C.; Plowright, A.A.; Tooke, T.R.; Christen, A.; Aven, N. Invasive Shrub Mapping in an Urban Environment from Hyperspectral and LiDAR-Derived Attributes. *Front. Plant Sci.* **2016**, *07*. [CrossRef] [PubMed]
34. Verrelst, J.; Geerling, G.W.; Sykora, K.V.; Clevers, J.G.P.W. Mapping of Aggregated Floodplain Plant Communities Using Image Fusion of CASI and LiDAR Data. *Int. J. Appl. Earth Obs. Geoinf.* **2009**, *11*, 83–94. [CrossRef]
35. Rajah, P.; Odindi, J.; Mutanga, O. Evaluating the Potential of Freely Available Multispectral Remotely Sensed Imagery in Mapping American Bramble (Rubus Cuneifolius). *S. Afr. Geogr. J.* **2018**, *100*, 291–307. [CrossRef]
36. Shezi, I.Z.; Poona, N.K. *An Investigation into Using Different Satellite Remote Sensors and Techniques to Identify, Map, Monitor and Predict the Spread and Distribution of Some of the Major Current and Emerging Invasive Alien Plant Species in KwaZulu-Natal*; Invasive Alien Plant Species Project; UKZN/DEA; School of Environmental Sciences, University of KwaZulu-Natal, Howard College Campus: Durban, South Africa, 2010.
37. Song, S.; Gong, W.; Zhu, B.; Huang, X. Wavelength Selection and Spectral Discrimination for Paddy Rice, with Laboratory Measurements of Hyperspectral Leaf Reflectance. *ISPRS J. Photogramm. Remote Sens.* **2011**, *66*, 672–682. [CrossRef]
38. Arafat, S.M.; Aboelghar, M.A.; Ahmed, E.F. Crop Discrimination Using Field Hyper Spectral Remotely Sensed Data. *Adv. Remote Sens.* **2013**, *2*, 63–70. [CrossRef]

39. Avola, G.; Di Gennaro, S.F.; Cantini, C.; Riggi, E.; Muratore, F.; Tornambè, C.; Matese, A. Remotely Sensed Vegetation Indices to Discriminate Field-Grown Olive Cultivars. *Remote Sens.* **2019**, *11*, 1242. [CrossRef]
40. Zagajewski, B.; Tømmervik, H.; Bjerke, J.W.; Raczko, E.; Bochenek, Z.; Kłos, A.; Jarocińska, A.; Lavender, S.; Ziółkowski, D. Intraspecific Differences in Spectral Reflectance Curves as Indicators of Reduced Vitality in High-Arctic Plants. *Remote Sens.* **2017**, *9*, 1289. [CrossRef]
41. Sławik, Ł.; Niedzielko, J.; Kania, A.; Piórkowski, H.; Kopeć, D. Multiple Flights or Single Flight Instrument Fusion of Hyperspectral and ALS Data? A Comparison of Their Performance for Vegetation Mapping. *Remote Sens.* **2019**, *11*, 970. [CrossRef]
42. Braun-Blanquet, J. *Pflanzensoziologie. Grundzüge der Vegetationskunde*, 3rd ed.; Springer-Verlag: Vienna, Austria, New York, NY, USA, 1964. [CrossRef]
43. RIEGL-RiPROCESS. Available online: http://www.riegl.com/products/software-packages/riprocess/ (accessed on 22 December 2020).
44. Terrasolid Software. Available online: https://www.terrasolid.com/ssl/download_software.php (accessed on 12 May 2020).
45. HySpex. Available online: https://www.hyspex.com/ (accessed on 18 December 2020).
46. PARGE Airborne Image Rectification. Available online: https://www.rese-apps.com/software/parge/index.html (accessed on 18 December 2020).
47. Richter, R.; Schlapfer, D. *Atmospheric/Topographic Correction for Airborne Imagery*; DLR report DLR-IB 565-02/14: Wessling, Germany, 2014.
48. OrthoVista. Available online: http://www.amigooptima.com/trimble-inpho/ortho-vista.php (accessed on 18 December 2020).
49. BCAL Lidar Tools. Available online: https://www.boisestate.edu/bcal/tools-resources/bcal-lidar-tools/ (accessed on 11 May 2020).
50. Pfeifer, N.; Mandlburger, G.; Otepka, J.; Karel, W. OPALS—A Framework for Airborne Laser Scanning Data Analysis. *Comput. Environ. Urban Syst.* **2014**, *45*, 125–136. [CrossRef]
51. Bhosale, N.; Manza, R.; Kale, K.V. Analysis of Effect of Gaussian, Salt and Pepper Noise Removal from Noisy Remote Sensing Images. In *Second International Conference on Emerging Research in Computing, Information, Communication and Applications (ERCICA 2014)*; Elsevier: Amsterdam, The Netherlands, 2014.
52. Shahdoosti, H.R.; Mirzapour, F. Spectral–Spatial Feature Extraction Using Orthogonal Linear Discriminant Analysis for Classification of Hyperspectral Data. *Eur. J. Remote Sens.* **2017**, *50*, 111–124. [CrossRef]
53. R Core Team. *R: The R Project for Statistical Computing*; R Foundation for Statistical Computing: Vienna, Austria, 2018.
54. Kuhn, M.; Wing, J.; Weston, S.; Williams, A.; Keefer, C.; Engelhardt, A.; Cooper, T.; Mayer, Z.; Kenkel, B.; R Core Team; et al. *Caret: Classification and Regression Training*; R Foundation for Statistical Computing: Vienna, Austria, 2018.
55. Weihs, C.; Ligges, U.; Luebke, K.; Raabe, N. KlaR Analyzing German Business Cycles. In *Data Analysis and Decision Support*; Baier, D., Decker, R., Schmidt-Thieme, L., Eds.; Springer: Berlin/Heidelberg, Germany, 2005; pp. 335–343. [CrossRef]
56. Oksanen, J.; Blanchet, F.G.; Kindt, R.; Legendre, P.; Minchin, P.; O'Hara, R.; Simpson, G.; Solymos, P.; Stevenes, M.; Wagner, H. *Vegan: Community Ecology Package*; R Package Version 2.5-6; R Foundation for Statistical Computing: Vienna, Austria, 2019.
57. Jensen, J.R. Biophysical Remote Sensing. *Ann. Assoc. Am. Geogr.* **1983**, *73*, 111–132. [CrossRef]
58. Kopeć, D.; Sabat-Tomala, A.; Michalska-Hejduk, D.; Jarocińska, A.; Niedzielko, J. Application of Airborne Hyperspectral Data for Mapping of Invasive Alien Spiraea Tomentosa L.: A Serious Threat to Peat Bog Plant Communities. *Wetl. Ecol. Manag.* **2020**, *28*, 357–373. [CrossRef]
59. Axelsson, A.; Lindberg, E.; Olsson, H. Exploring Multispectral ALS Data for Tree Species Classification. *Remote Sens.* **2018**, *10*, 183. [CrossRef]
60. Ørka, H.O.; Næsset, E.; Bollandsås, O.M. Classifying Species of Individual Trees by Intensity and Structure Features Derived from Airborne Laser Scanner Data. *Remote Sens. Environ.* **2009**, *113*, 1163–1174. [CrossRef]
61. Komárek, J.; Klouček, T.; Prošek, J. The Potential of Unmanned Aerial Systems: A Tool towards Precision Classification of Hard-to-Distinguish Vegetation Types? *Int. J. Appl. Earth Obs. Geoinf.* **2018**, *71*, 9–19. [CrossRef]
62. Prošek, J.; Šímová, P. UAV for Mapping Shrubland Vegetation: Does Fusion of Spectral and Vertical Information Derived from a Single Sensor Increase the Classification Accuracy? *Int. J. Appl. Earth Obs. Geoinf.* **2019**, *75*, 151–162. [CrossRef]
63. De Luca, G.; Silva, J.M.N.; Cerasoli, S.; Araújo, J.; Campos, J.; Di Fazio, S.; Modica, G. Object-Based Land Cover Classification of Cork Oak Woodlands Using UAV Imagery and Orfeo ToolBox. *Remote Sens.* **2019**, *11*, 1238. [CrossRef]
64. Wang, L.; Wei, Y. Revised Normalized Difference Nitrogen Index (NDNI) for Estimating Canopy Nitrogen Concentration in Wetlands. *Optik* **2016**, *127*, 7676–7688. [CrossRef]
65. Liang, L.; Di, L.; Huang, T.; Wang, J.; Lin, L.; Wang, L.; Yang, M. Estimation of Leaf Nitrogen Content in Wheat Using New Hyperspectral Indices and a Random Forest Regression Algorithm. *Remote Sens.* **2018**, *10*, 1940. [CrossRef]
66. Ellenberg, H.; Weber, H.E.; Düll, R.; Wirth, W.; Werner, W.; Paulißen, D. Zeigerwerte von Pflanzen in Mitteleuropa. *Scr. Geobot.* **1992**, *18*, 1–248.
67. Strik, B.C. Seasonal Variation in Mineral Nutrient Content of Primocane-Fruiting Blackberry Leaves. *HortScience* **2015**, *50*, 540–545. [CrossRef]
68. Hornero, A.; Hernández-Clemente, R.; North, P.R.J.; Beck, P.S.A.; Boscia, D.; Navas-Cortes, J.A.; Zarco-Tejada, P.J. Monitoring the Incidence of Xylella Fastidiosa Infection in Olive Orchards Using Ground-Based Evaluations, Airborne Imaging Spectroscopy and Sentinel-2 Time Series through 3-D Radiative Transfer Modelling. *Remote Sens. Environ.* **2020**, *236*, 111480. [CrossRef]

69. Ponder, A.; Hallmann, E. Phenolics and Carotenoid Contents in the Leaves of Different Organic and Conventional Raspberry (Rubus Idaeus L.) Cultivars and Their In Vitro Activity. *Antioxidants* **2019**, *8*, 458. [CrossRef]
70. Thorp, K.R.; French, A.N.; Rango, A. Effect of Image Spatial and Spectral Characteristics on Mapping Semi-Arid Rangeland Vegetation Using Multiple Endmember Spectral Mixture Analysis (MESMA). *Remote Sens. Environ.* **2013**, *132*, 120–130. [CrossRef]
71. Serbin, G.; Hunt, E.R., Jr.; Daughtry, C.S.T.; McCarty, G.W. Assessment of Spectral Indices for Cover Estimation of Senescent Vegetation. *Remote Sens. Lett.* **2013**, *4*, 552–560. [CrossRef]
72. Wu, W. The Generalized Difference Vegetation Index (GDVI) for Dryland Characterization. *Remote Sens.* **2014**, *6*, 1211–1233. [CrossRef]
73. Solano, F.; Di Fazio, S.; Modica, G. A Methodology Based on GEOBIA and WorldView-3 Imagery to Derive Vegetation Indices at Tree Crown Detail in Olive Orchards. *Int. J. Appl. Earth Obs. Geoinf.* **2019**, *83*, 101912. [CrossRef]
74. Rizeei, H.M.; Shafri, H.Z.M.; Mohamoud, M.A.; Pradhan, B.; Kalantar, B. Oil Palm Counting and Age Estimation from WorldView-3 Imagery and LiDAR Data Using an Integrated OBIA Height Model and Regression Analysis. *J. Sens.* **2018**, *2018*, 2536327. Available online: https://www.hindawi.com/journals/js/2018/2536327/ (accessed on 25 December 2020). [CrossRef]
75. Varin, M.; Chalghaf, B.; Joanisse, G. Object-Based Approach Using Very High Spatial Resolution 16-Band WorldView-3 and LiDAR Data for Tree Species Classification in a Broadleaf Forest in Quebec, Canada. *Remote Sens.* **2020**, *12*, 3092. [CrossRef]
76. Niphadkar, M.; Nagendra, H. Remote Sensing of Invasive Plants: Incorporating Functional Traits into the Picture. *Int. J. Remote Sens.* **2016**, *37*, 3074–3085. [CrossRef]